This is a repository copy of *Subthreshold diode characteristics of InAs/GaAs quantum dot lasers*.

White Rose Research Online URL for this paper:
http://eprints.whiterose.ac.uk/97410/

Version: Accepted Version

Article:

Spencer, P., Clarke, E., Murray, R. et al. (3 more authors) (2011) Subthreshold diode characteristics of InAs/GaAs quantum dot lasers. Physical review B: Condensed matter and materials physics, 83 (20). 205407. ISSN 1098-0121

https://doi.org/10.1103/PhysRevB.83.205407

Reuse
Unless indicated otherwise, fulltext items are protected by copyright with all rights reserved. The copyright exception in section 29 of the Copyright, Designs and Patents Act 1988 allows the making of a single copy solely for the purpose of non-commercial research or private study within the limits of fair dealing. The publisher or other rights-holder may allow further reproduction and re-use of this version - refer to the White Rose Research Online record for this item. Where records identify the publisher as the copyright holder, users can verify any specific terms of use on the publisher's website.

Takedown
If you consider content in White Rose Research Online to be in breach of UK law, please notify us by emailing eprints@whiterose.ac.uk including the URL of the record and the reason for the withdrawal request.

eprints@whiterose.ac.uk
https://eprints.whiterose.ac.uk/

Sub-threshold diode characteristics of InAs/GaAs quantum dot lasers

P. Spencer, E. Clarke, R. Murray

Physics Department, Imperial College London, Blackett Laboratory, Prince Consort Road, London SW7 2AZ, U. K.

K. M. Groom, R. R. Alexander, R. A. Hogg

EPSRC National Centre for III-V Technologies, University of Sheffield, Centre for Nanoscience & Technology, North Campus, Broad Lane, Sheffield S3 7HQ, U. K.

Abstract

The temperature dependence of the carrier dynamics in ensembles of InAs/GaAs quantum dots (QDs) are of interest, both from a fundamental point of view but also because of the consequences for the performance of QD-based optoelectronic devices. While this topic has been studied before using optical techniques, here we approach the topic by analyzing the current-voltage (IV) characteristic of QD diodes. Using a current-modulation technique, the transition from “trap-like” to “thermalized” behavior as the temperature is raised from 80 K to room-temperature is observed. Furthermore, the results suggest that the IV curve is sensitive to the separate escape of electrons and holes and the intersubband spacing of the electron states and that of the hole states is estimated from the data.

I. INTRODUCTION

InAs/GaAs quantum dots (QD) have received much attention for their potential use in next-generation telecoms light sources [1]. QD-based lasers were predicted to have low, temperature-insensitive threshold currents [2, 3] but this requires large energy separations between the discrete QD states to suppress thermal effects. At low temperatures QD devices do indeed exhibit close to ideal characteristics, but by room temperature their performance is consistent with thermal spreading across available energy states with critical temperature values not significantly better than quantum well lasers [4-6]. In this paper we show that using electrical measurements of the diode behavior of QD lasers operating well below the lasing threshold, we can obtain valuable additional information on the transfer of carriers across the diode across a wide temperature range. Our results are consistent with a gradual onset of carrier thermalization in the QD ensemble with increasing temperature, as expected, but also show that there is independent escape of holes and electrons in the mid-temperature range.

II. SAMPLE DETAILS

The devices studied here were processed from a QD laser structure containing three QD bilayers [7], in a standard laser diode design grown by molecular beam epitaxy on an (100) GaAs substrate. The QD bilayers comprise two closely-stacked QD layers, separated by 10 nm GaAs: a seed layer that determines the overall QD density and an upper layer, for which the growth conditions can then be chosen to provide a significant extension in the emission wavelength. The two QD layers are sufficiently close together to allow efficient carrier transfer from the seed layer to the upper layer, such that emission from the seed layer is suppressed and device operation is

determined by the upper layer QDs [7, 8]. The active region is an undoped 500 nm thick layer of GaAs containing three QD bilayers separated by 50 nm bounded by n and p-doped 1500 nm thick $Al_{0.33}Ga_{0.67}As$ cladding layers. Each bilayer was grown on a GaAs surface that had been annealed at 580 °C for ten minutes; 2.4 monolayers (ML) of InAs was deposited at a growth rate of 0.014 MLs^{-1} and a temperature of 480 °C to form the seed layer, resulting in an areal QD density of 2.7 x 10^{10} cm^{-2}, measured by atomic force microscopy on an uncapped sample. The QDs were then buried by a 10 nm GaAs cap, grown at the same temperature, followed by another anneal step at 580 °C for ten minutes. The upper QD layer was then grown by depositing 3.3 ML of InAs at the same growth rate but a reduced temperature of 467 °C. The upper-layer was buried by 15 nm of GaAs at the same temperature before increasing the temperature to 580 °C for subsequent growth. The upper cladding layer was followed by 50 nm of GaAs Be-doped to 6 x 10^{17} cm^{-3} with a 350 nm thick GaAs contact layer doped to 1 x 10^{19} cm^{-3}. Devices were processed into ridge waveguides, etching to within 100 nm of the active region. After etching, an AuZnAu Ohmic contact was evaporated then annealed at 360 °C to form the anode. A 500nm SiN insulating layer was used to isolate the sidewalls and TiAu contact pads adjacent to the ridge were evaporated, and then electroplated with several µm of Au. The cathode was formed by depositing an InGeAu Ohmic back contact after the substrate had been thinned to ~100 µm. The contacts were annealed at 360 °C to achieve low-resistance Ohmic contacts. The samples were then cleaved into 5 mm-long lasers: Samples A and B were 15 µm wide devices while sample C was 5 µm wide. The electroluminescence (EL) spectrum is shown in figure 1. It shows clearly resolved room-temperature ground-state (GS) emission at E_{GS} = 924.2 ± 0.1 meV and first excited state (X1) emission at E_{X1} = 984.5 ± 0.2 meV, giving a state separation

$\Delta E = 60.3 \pm 0.3$ meV. For the IV measurements temperature control was provided by mounting the samples in a closed cycle helium cryostat.

III. MEASUREMENTS

A. Switch-on voltage

The current I through a non-degenerate diode should scale exponentially as an applied voltage is increased relative to the barrier potential. Here we investigate the diode behavior well below threshold and monitor the "switch-on voltage" V_{on} obtained at a bias current of $I_{on} = 2$ mA for a range of temperatures. The results are shown in figure 3(a). The effect of series resistance was neglected since it is less than 2 Ω for these samples, resulting in an error of <4 mV, or less than 0.5 % of V_{on}. The data show that V_{on} is close to the potential of the GaAs energy-gap of ~1.5 V (E_{GaAs}/q) at low temperatures, while above 150 K it falls towards E_{GS}/q as it approaches room temperature. We attribute the low-temperature value to non-thermalization of the dots which in this instance act as mid-gap traps; captured carriers cannot escape but can recombine resulting in some spontaneous light emission and the effective barrier is that due to the GaAs matrix. The situation is reversed at room temperature where carriers are constantly captured by the QDs but are also able to escape and thermalize with the GaAs matrix, establishing quasi-Fermi levels that lie close to the dot GS. We shall now show that the diode characteristic of the QD lasers can give further insight into these details by offering a way to distinguish "trap-like" from "ideal" band-to-band recombination.

B. Ideality factor

The IV characteristics of a diode are usually described by the ideal diode approximation as a function of I and the junction voltage V_j, where η is the ideality factor and I_S is the saturation current, as shown in equation 1 [9]:

$$I = I_S\left[\exp\left(\frac{qV_j}{\eta k_B T}\right) - 1\right] \qquad (1)$$

This equation can be derived analytically for some simplified cases but, in general, a proper solution requires numerical calculation. However, it does provide a useful empirical tool for analyzing experimental IV curves. The IV curve of a diode operated in DC under forward-bias can be written as the series sum of V_j for an ideal diode and the series resistance R as shown in equation 2, where V is the voltage measured at the diode contacts.

$$V = V_j + IR = \frac{\eta k_B T}{q}\ln\left(\frac{I}{I_S} + 1\right) + IR \qquad (2)$$

Measuring η in the presence of a series resistance R is known to be difficult, so we have employed a current modulation measurement to extract η [10, 11]. We chose to measure d^2V/dI^2 because an Ohmic series resistance has no second derivative with respect to current. To achieve this, the bias current was modulated with a superposition of two sine waves at ~15 kHz and ~16 kHz. A lock-in amplifier then measured the second-derivative of the IV curve by detecting the voltage response of the diode at the difference frequency of 1 kHz. This frequency-mixing technique is crucial in order to avoid harmonic distortion in the drive circuits, which would cause the lock-in to measure a combination of the first and second derivatives. This is particularly important since the second derivative falls off as $1/I^2$, quickly becoming small as the bias is increased, while the first derivative only falls off as 1/I. To ease interpretation, the second derivative data from the lock-in was then multiplied by a

pre-factor $-I^2$, which allows small changes in the junction voltage to be identified. Applying this treatment to (2) gives (3), which, in the limit of $I_S << I$, reduces to a constant voltage signal.

$$-I^2 \frac{d^2V}{dI^2} \approx \frac{\eta k_B T}{q} \frac{I^2}{(I+I_S)^2} \xrightarrow{\lim I_S << I} \frac{\eta k_B T}{q} \quad (3)$$

Figure 2 shows a $-I^2d^2V/dI^2$ measurement obtained at room temperature from a reference Schottky diode and one of the QD laser diodes (sample A). Ignoring the data obtained at very low currents, the Schottky diode exhibits a constant value of $\frac{\eta k_B T}{q} \approx 25\,\mathrm{mV}$, consistent with an ideality factor η~1 as expected. The QD laser diode shows more complicated behavior with a constantly rising background (which we observe for all QD devices including those grown by other groups) and a peak around 150 mA which coincides with the lasing threshold [12]. Here we extrapolate the data to give an intercept voltage equal to $\eta k_B T/q$ from which we can extract a value for η which is then used to indicate the detailed nature of the diode. Figure 3(b) shows the temperature dependence of η from 80 K to 300 K. At low temperatures η~2, consistent with "trap-like" recombination via the QDs, whilst at high-temperatures η tends to unity, consistent with thermalized band-to-band recombination in the QDs. At intermediate temperatures, η rises to a peak value of ~4 around 150 K. Such high values of η have no obvious text-book interpretation but the peak does imply that there is no monotonic transition from trap-like to thermalized QDs and must involve an intermediate regime [13]. Remembering that QD lasers are bipolar devices involving both electrons and holes carrier escape can occur in either pair-wise fashion (geminate) or separately for each species (non-geminate). The intermediate regime may therefore be a symptom of the non-geminate escape of one

carrier-species, as has already been inferred from optical data [14]. To resolve this it is necessary to analyze I_S.

C. Saturation current

In an ideal diode, I_S can be said to represent the diffusion current that would flow across the diode junction at thermal equilibrium if it were not opposed by the built-in electric field; it is often described as the theoretical reverse-bias leakage current (in the absence of defects and shunt resistances) since, to a first approximation, the diffusion current does not change under electric field. In the heterostructure considered here, the high-bandgap AlGaAs barriers mean that there is negligible diffusion across the junction compared to the thermally-generated carriers that escape the intrinsic layer (in the form of electrons into the n-type side and holes into the p-type side), therefore in this case we assume I_S is entirely described by the thermal generation and recombination of carriers in the active region. Specifically, we consider it here as the net generation of carriers that can escape the active region without recombining. Empirically, a small I_S means a higher V_{on} because the thermal generation of carriers is smaller when the energy-gap is higher and conversely a high I_S means a small V_{on}. I_S can be estimated from the data by re-arranging equation (2) to obtain (4), substituting the measured V_{on} and η, while again neglecting R.

$$I_S = \frac{I_{on}}{\exp\left(\frac{qV_{on}}{\eta k_B T}\right) - 1} \quad (4)$$

I_S, as deduced from V_{on} and η, is plotted in figure 4. The data suggests that below 150 K carrier escape is negligible and the QDs act as efficient traps for any electrons and holes in the active region, so carrier recombination dominates over generation, resulting in a small I_S. In this regime, carriers captured from the GaAs matrix by the QDs will recombine eventually and so the capture process appears analogous to

recombination from a thermalized carrier population in the GaAs matrix. As the temperature is raised through the transition region of high η, I_S rises sharply to a peak at ~190 K and then falls as the temperature is further raised. We attribute this to the non-geminate escape of holes and electrons. The lower confinement of the holes allows them to escape at lower temperatures than the electrons, leading to the rise in I_S with temperature seen in figure 4, as more of the thermally-generated carriers become able to escape the active region. These holes do not recombine in the active region because of the low availability of electrons, which are still efficiently trapped by the QDs. As the temperature is raised further and the electrons are able to escape, the active region is populated with both electrons and holes, as a result the thermally-generated carriers are able to recombine before leaving the junction region, causing I_S to drop with further increases in temperature.

IV. EFFECTIVE BARRIER HEIGHT

At this point, the expectation that the holes escape at lower temperatures than the electrons is purely based on their lower confinement energy compared to that of the electrons [15, 16]. We will now proceed with a more detailed analysis of I_S and η in an attempt to gain more quantitative insight, by using these parameters to infer the "effective" barrier height of the diode junction. An effective barrier height would describe the rate-determining potential barrier within the diode, as opposed to the overall potential barrier V_{on} (similar to differential resistance as opposed to pure Ohmic resistance). To estimate this quantity from the data in figure 4, we note that qV_{on}/η is always significantly larger than k_BT allowing equation (4) to be approximated as (5):

$$I_S \approx I_{on} \exp\left(\frac{-qV_{on}}{\eta k_B T}\right) \qquad (5)$$

Equation (6) can then be substituted into the ideal diode equation (1) to give (6). This suggests that the switch-on voltage divided by the ideality factor specifies the size of the rate-determining potential barrier.

$$I \approx I_{on} \exp\left(\frac{qV_j/\eta - qV_{on}/\eta}{k_B T}\right) \tag{6}$$

Therefore, a diode requires a voltage of the order of V_{on} to conduct but the variation of current, for a change in applied voltage, is determined by the smaller term qV_{on}/η. In an ideal Schottky diode (η=1) recombination occurs with no internal structure to the process (i.e. pure band-to-band), so a higher η gives details of any internal structure to the recombination pathways of the non-degenerate diode. For instance, the limiting case of Shockley-Read-Hall (SRH) recombination involves a mid-gap state which must alternatively capture electrons and holes to achieve interband recombination. In this case, the presence of the mid-gap trap state halves the rate-determining potential barrier compared to the ideal case and this gives $\eta = 2$. SRH theory thus gives ideality factors between 1 and 2 depending on the balance of rates between ideal and trap-mediated recombination. Diodes with $\eta > 2$ have frequently been reported, especially for wide bandgap materials such as GaN and ZnO, and has been attributed to coupled defect levels [17], variation in Schottky barrier height [18, 19], the combination of ideality factors of a series of diode junctions within a structure [20, 21] or localized (Frenkel-Poole) conduction in amorphous layers or at interfaces [22].

The results of this analysis are plotted on an Arrhenius scale in the inset to figure 4 and the trend in qV_{on}/η can be fitted with the sum of two Arrhenius-like dependencies (equation 7), with table 1 giving the fitted parameters for samples A, B and C.

$$\frac{qV_{on}}{\eta} = A\exp\left(\frac{E_0}{k_B T}\right) + B\exp\left(\frac{-E_1}{k_B T}\right) \quad (7)$$

Below 160 K, qV_{on}/η reduces with activation energy $E_0 = 15.2 \pm 0.1$ meV, while at temperatures above 160 K it rises with activation energy $E_1 = 58.3 \pm 0.8$ meV (the actual slope of the trend being $E_1 - E_0 = 43.1$ meV in this region). The energy-splitting of the GS and X1 emission is believed to be shared between the electrons and holes with a band offset ratio of ~2.5:1 [16, 23-24], respectively, giving an expected electron-state spacing of $\Delta E_E \sim 43$ meV and a hole-state spacing of $\Delta E_H \sim 17$ meV; from previous optical studies this spacing is consistent amongst the first few confined-states of the QDs [15, 16]. We attribute E_0 and E_1 to the activation energies required for scattering between the hole states (E_0) and both the electron and hole states (E_1) in the QDs. The use of Arrhenius relations in fitting the data is justified by assuming the behavior of the diode junction is determined by the rate of intradot carrier scattering between the confined-states. We believe this presents strong evidence that the high ideality factor in the "intermediate regime" is due to the separate escape of holes at a lower temperature than the electrons.

V. CONCLUSION

By comparison of the temperature dependence of the switch-on voltage, ideality factor and saturation current behavior of InAs/GaAs QD bilayer laser diodes with ideal diode behavior, it was found that the quasi-Fermi levels of the diodes are associated with the GaAs/WL continuum states at low temperatures, but drop into the QD confined-states as carrier escape becomes possible at higher temperatures and carrier thermalization occurs. A peak in the ideality factor around 150 K suggests that the transition from "trap-like" recombination at low temperatures to thermalized recombination above room-temperature is not a single phase-transition. We propose

that the ideality factor of the QD diode can be interpreted in terms of internal structure to the recombination pathways and thus the rate-determining barrier within the QD junction can be analyzed. We have proposed a physical model to explain the barrier energy in terms of the rate-determining processes being: (a) one-way carrier capture into the QDs at low temperature, (b) partial thermalization of the holes only near 160 K and (c) interband recombination across a thermalized QD GS at high-temperatures, once both carrier species can escape.

References

1. D. J. Mowbray and M. S. Skolnick, J. Phys. D: Appl. Phys. **38**, 2059 (2005)
2. M. Asada, Y. Miyamoto, Y. Suematsu, IEEE J. Quantum Electron. **22**, 1915 (1986)
3. Y. Arakawa, H. Sakaki, Appl. Phys. Lett. **40**, 939 (1982)
4. H. D. Summers, J. D. Thomson, P. M. Smowton, P. Blood, M. Hopkinson, Semicond. Sci. Technol. **16**, 140 (2001)
5. I. O'Driscoll, P. M. Smowton, P. Blood, IEEE J. Quantum Electron. **45**, 380 (2009)
6. I. O'Driscoll, P. Blood, P. M. Smowton IEEE J. Quantum Electron. **46**, 525 (2010)
7. E. C. Le Ru, P. Howe, T. S. Jones, R. Murray, Phys. Rev. B **67**, 165303 (2003)
8. E. Clarke, P. Howe, M. Taylor, P. Spencer, E. Harbord, R. Murray, S. Kadkhodazadeh, D. W. McComb, B. J. Stevens, R. A. Hogg, J. Appl. Phys. **107**, 113502 (2010)
9. S. Sze, K. K. Ng, "Physics of Semiconductor Devices", Wiley-Blackwell (2006)
10. T. L. Paoli, IEEE Trans. Electron. Devices **23**, 1333 (1976)
11. T. L. Paoli, J. F. Svacek, Rev. Sci. Instrum. **47**, 1016 (1976)
12. P. Spencer, E. Clarke, P. Howe, R. Murray, Electron. Lett. **43**, 574 (2007)
13. S. Sanguinetti, M. Henini, M. Grassi Alessi, M. Capizzi, P. Frigeri, S. Franchi, Phys. Rev. B **60**, 8276 (1999)
14. E. C. Le Ru, J. Fack, R. Murray, Phys. Rev. B **67**, 245318 (2003)
15. R. J. Warburton, C. S. Dürr, K. Karrai, J. P. Kotthaus, G. Medeiros-Ribeiro, P. M. Petroff, Phys. Rev. Lett. **79**, 5282 (1997)
16. B. N. Murdin, A. R. Hollingworth, J. A. Barker, D. G. Clarke, P. C. Findlay, C. R. Pidgeon, J.-P. R. Wells, I. V. Bradley, S. Malik, R. Murray, Phys. Rev. B **62**, R7755 (2000)
17. A. Schenk, U. Krumbein, J. Appl. Phys. **78**, 3185 (1995)
18. E. H. Rhoderick, R. H. Williams Metal-Semiconductor Contacts (Oxford University Press, Oxford, 1988)
19. S. Chand, J. Kumar, J. Appl. Phys. **82**, 5005 (1997)
20. J. M. Shah, Y.-L. Li, Th. Gessmann, E. F. Schubert, J. Appl. Phys. **94**, 2627 (2003)

21. C.-X. Wang, G.-W. Yang, H.-W. Liu, Y.-H. Han, J.-F. Luo, C.-X. Gao, G.-T. Zou, Appl. Phys. Lett. **84**, 2427 (2004)
22. M. Brötzmann, U. Vetter, H. Hofsäss, J. Appl. Phys. **106**, 063704 (2009)
23. R. J. Warburton, B. T. Miller, C. S. Dürr, C. Bödefeld, K. Karrai, J. P. Kotthaus, G. Medeiros-Ribeiro, P. M. Petroff, and S. Huant, Phys. Rev. B **58**, 16221 (1998).
24. M. Fricke, A. Lorke, J. P. Kotthaus, G. Medeiros-Ribeiro, and P. M. Petroff, Europhys. Lett. **36**, 197 (1996)

Table I

	E_0 (meV)	E_1 (meV)
Sample A	19.4 ± 0.3	48.7 ± 0.8
Sample B	16.8 ± 0.2	60.1 ± 0.9
Sample C	9.3 ± 0.2	66 ± 2
Average	**15.2 ± 0.1**	**58.3 ± 0.8**

Figure Captions

Table 1: Activation energies E_0 and E_1 for samples A, B and C; we attribute E_0 and E_1-E_0 to the energy spacing between the confined hole and electron states, respectively, within the QDs.

Figure 1: Electroluminescence spectrum of the QD bilayer laser below threshold at room-temperature. The GS emission peak is at 1341 nm and the X1 emission peak is at 1259 nm; the GS and X1 emission is separated by 60.3 ± 0.3 meV.

Figure 2: An example IV curve and $-I^2d^2V/dI^2$ spectrum of the QD laser diode. While the latter is different from the expected form of an ideal diode (e.g. the Schottky diode shown as a dotted line) diode, there is still a clear intercept voltage from which the ideality can be deduced.

Figure 3: (a) The temperature dependence of the switch-on voltage. At low temperatures it is close to the GaAs bandgap potential, while near room-temperature it is associated with the QD GS energy. (b) The temperature dependence of the ideality factor, extracted from the current modulation measurement. The ideality factor is high at low-temperature, peaking near 150 K before dropping towards unity at high temperatures.

Figure 4: I_S calculated from V_{ON} and η. It is suppressed below 150 K because of the efficient capture of carriers into the non-thermal QD states, while at higher temperatures it is thermalized. (Inset) Arrhenius plot of the estimated rate-determining barrier energy $\phi_{barrier}$ together with fit-lines as described in the text.

Figure 1

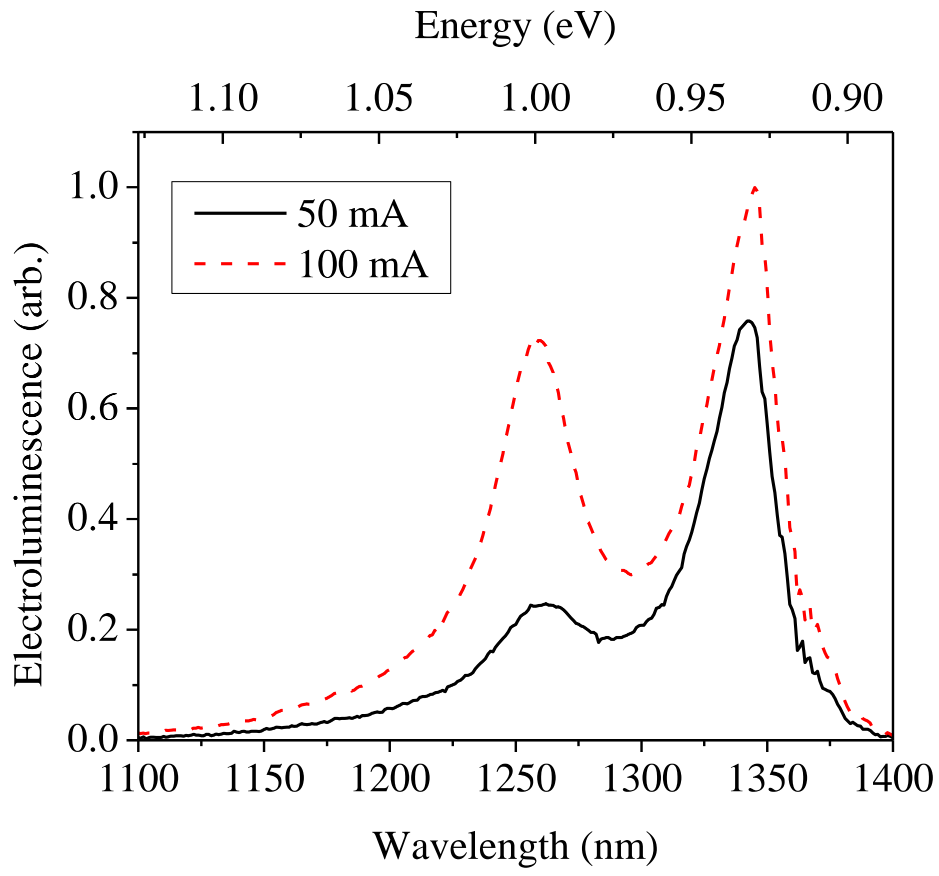

Figure 2

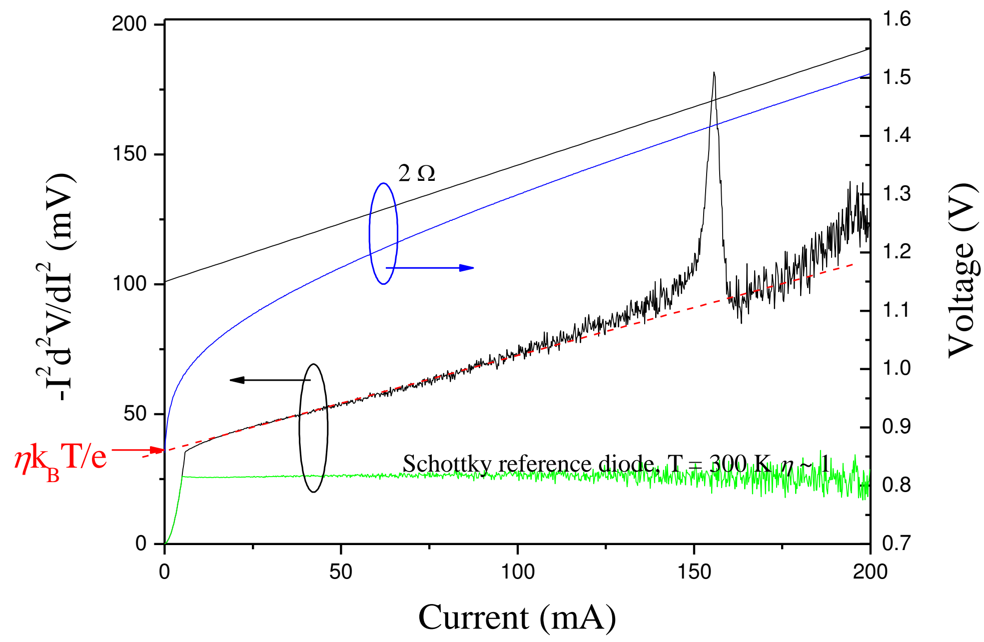

Figure 3

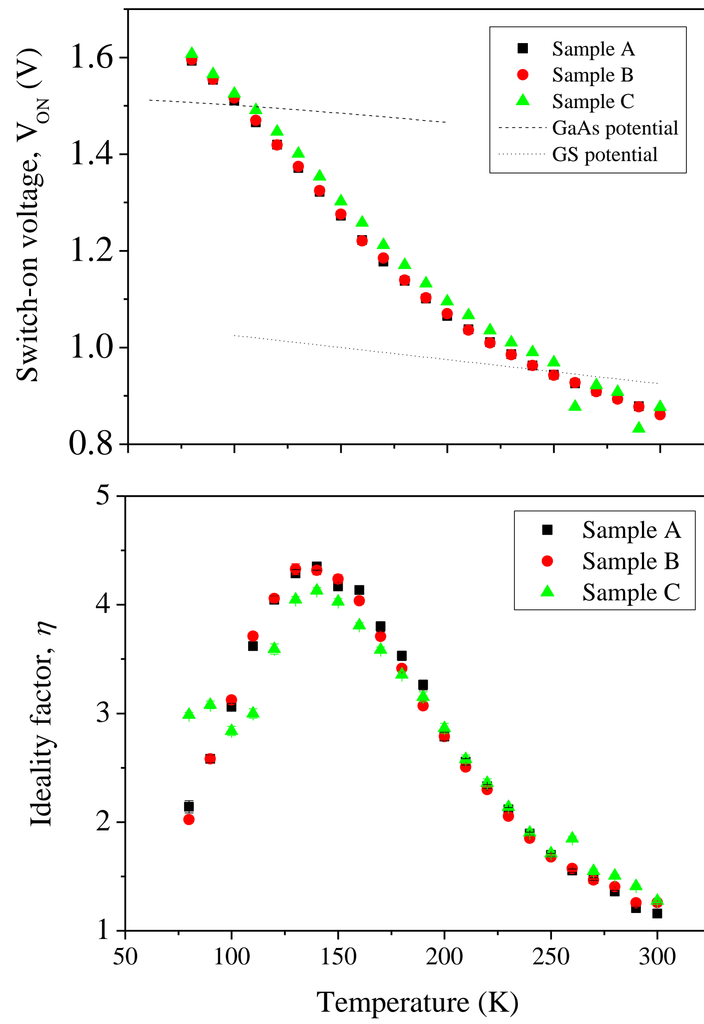

Figure 4